ELSEVIER

Contents lists available at ScienceDirect

Photoacoustics

journal homepage: www.elsevier.com/locate/pacs





Compressible viscoelasticity of cell membranes determined by gigahertz-frequency acoustic vibrations

Kuai Yu^a, Yiqi Jiang^b, Yungao Chen^b, Xiaoyan Hu^c, Junlei Chang^c, Gregory V. Hartland^d, Guo Ping Wang^{a,*}

- a State Key Laboratory of Radio Frequency Heterogeneous Integration, College of Electronics and Information Engineering, Shenzhen University, Shenzhen 518060, China
- ^b Institute of Microscale Optoelectronics, Shenzhen University, Shenzhen 518060, China
- c Institute of Biomedicine and Biotechnology, Shenzhen Institute of Advanced Technology, Chinese Academy of Sciences, Shenzhen 518055, China
- ^d Department of Chemistry and Biochemistry, University of Notre Dame, Notre Dame, Indiana 46556, USA

ARTICLE INFO

Keywords: Acoustic vibrations Cell membrane viscoelasticity Membrane fluid mechanics Structural relaxation time High-frequency biomechanics Au nanoplates

ABSTRACT

Membrane viscosity is an important property of cell biology, which determines cellular function, development and disease progression. Various experimental and computational methods have been developed to investigate the mechanics of cells. However, there have been no experimental measurements of the membrane viscosity at high-frequencies in live cells. High frequency measurements are important because they can probe viscoelastic effects. Here, we investigate the membrane viscosity at gigahertz-frequencies through the damping of the acoustic vibrations of gold nanoplates. The experiments are modeled using a continuum mechanics theory which reveals that the membranes display viscoelasticity, with an estimated relaxation time of ca. 5.7 + 2.4 / -2.7 ps. We further demonstrate that membrane viscoelasticity can be used to differentiate a cancerous cell line (the human glioblastoma cells LN-18) from a normal cell line (the mouse brain microvascular endothelial cells bEnd.3). The viscosity of cancerous cells LN-18 is lower than that of healthy cells bEnd.3 by a factor of three. The results indicate promising applications of characterizing membrane viscoelasticity at gigahertz-frequency in cell diagnosis.

1. Introduction

The cell membrane is a biological structure that physically separates the intracellular components from the extracellular environment, and protects the cell from its environment. Biological membranes contain a variety of molecules, notably lipids and proteins, and they form a lipid-protein bilayer structure through the process of self-assembly. Various membrane models were proposed to correlate the lipid-protein bilayer complexity and hierarchy to the dynamics and functions of cell membranes [1,2]. The fluid-mosaic membrane model represents the most popular accepted picture of biological membranes, where the cell membrane is a two-dimensional bilayer fluid, that enables individual lipids, lipid domains, embedded proteins, and molecular complexes to spatially reorganize and freely diffuse [3–5].

An important property of membranes is their biomechanics, which strongly regulates the transport of biomolecules both in-plane and out-of-plane of the membrane [6,7]. Since the earliest mechanical characterization of cell membranes, it has been noticed that viscosity of the

bilayer fluid leads to many important rheological behaviors [8,9]. Maintenance and modulation of cell membrane viscosity is thus essential for cell survival and changes of cellular states [1,10]. Moreover, accumulated evidence shows a link between cell membrane viscosity to various human diseases. For instance, Alzheimer's disease and metastatic behavior of cancerous cells are associated with a change in membrane viscosity [1]. Therefore, understanding and being able to measure and quantify such changes is both fundamentally interesting and can also provide insights into disease evolution.

For a biological membrane both the transport of biomolecules along the membrane and across the membrane are important. In the past few decades, methods have been developed to study the transport along the membrane, yielding information about in-plane viscosity of cell membranes [11,12]. It is much more challenging to measuring the viscosity corresponding to motion across the membrane due to the extremely thin membrane thicknesses [13–16]. Many of the available techniques require the application of physical stress to the cells, such as mechanical stretching, micropipette aspiration, microfluidics and optical tweezers,

E-mail address: gpwang@szu.edu.cn (G.P. Wang).

https://doi.org/10.1016/j.pacs.2023.100494

^{*} Corresponding author.

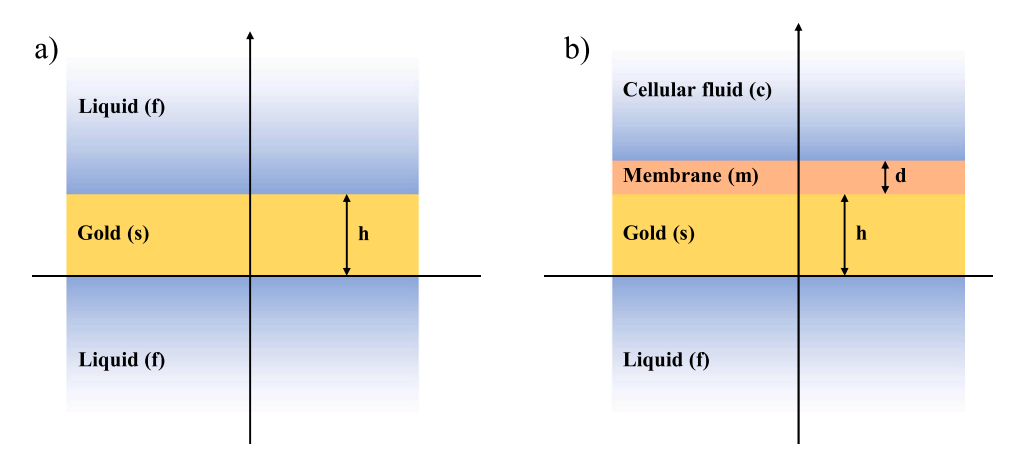


Fig. 1. Theoretical models of Au NPL vibrating in (a) a symmetrical liquid environment. (b) an unsymmetrical environment where the top surface of the Au NPL was covered by a lipidprotein bilayer membrane and cellular fluid. The Au NPL has thickness of $h \sim 20-30$ nm, and the membrane layer has thickness of $d \sim$ 4-10 nm.[52] The liquid can be PBS buffer solution or live cell culture medium. Note that the cellular fluid is different from the liquid. In this work the cellular fluid of live cells is treated as water due to their closed Brillouin frequencies at 7.3 ± 0.1 GHz. In our theoretical calculations, ~ 6 nm membrane average thickness was used. The values of liquid parameters in the continuum mechanics model are given in Supporting Information.

which have limited spatial resolution and cannot differentiate the in-plane and longitudinal responses of cell membranes [17–21]. Optical spectroscopy can measure the rheological behavior of cell membranes at high spatial resolution through fluorescence correlation spectroscopy and fluorescence lifetime imaging [22–26]. Neutron scattering and atomic force microscopy are capable of measuring the viscosity of cell membranes [27–31]. However, the response of cell membranes to deformation highly depends on the time scale and the above methods are relatively low frequency experiments. Acoustic Brillouin spectroscopy is well established in biomechanics and can probe viscous and viscoelastic properties of living cells at gigahertz-frequencies [7,32–36]. However, the acoustic wavelength is on the order of \sim 200 nm and far exceeds the membrane thickness of \sim 4–10 nm, and diffraction of the acoustic waves hinders the applications where high spatial resolution is needed [7,37].

In this study, we introduce a method to probe the compressible viscoelasticity of biological cell membranes at gigahertz-frequency by using coherent acoustic vibrations of ultra-thin gold nanoplates (Au NPLs). The coherent acoustic vibrations of Au NPLs were excited by femtosecond laser pulses. The vibrational profile consists of modulation of the plate thickness, which can periodically compress the attached cell membranes. By measuring the lifetimes of the acoustic vibrations of Au NPLs with and without cell membranes, the contribution from the cell membrane to the damping was determined. A continuum mechanics model was developed to calculate the damping of the Au NPL breathing modes due to the membrane. Comparison of the experimental data to the model shows that viscoelastic effects occur for membrane bilayers at gigahertz-frequency time scales, with a structural relaxation time of ca. 5.7 + 2.4 / -2.7 ps. The capability to measure membrane viscoelasticity further enabled us to differentiate cancerous cells (the human glioblastoma cells LN-18) from normal cells (the mouse brain microvascular endothelial cells bEnd.3). The results of softer and more fluid membrane property of cancerous cells are consistent with previous conclusions [38, 39]. Successful characterization of membrane viscoelasticity at gigahertz-frequency may provide a useful diagnostic biomarker for the development of therapeutics.

2. Results and discussion

2.1. Theoretical analysis of damping by viscoelastic membranes

Femtosecond laser excitation of metal nanoparticles causes rapid heating that can excite acoustic vibrational modes [40,41]. Vibrational frequencies and lifetimes are the two main characteristics for these modes. Single-particle pump-probe spectroscopy was used to measure the vibrational frequencies and lifetimes [42,43]. A typical vibrational trace of Au NPLs is shown in the Supporting Information. The

vibrational frequency provides information about the elastic property of the particles, and the vibrational lifetime reports on how the particles interact mechanically with their environment [44,45]. Normally, high-frequency acoustic modes have relatively low vibrational lifetimes which prevent the accurate measurements of environment damping. Recently, two-dimensional Au NPLs were shown to have breathing mode vibrations with long lifetimes and large quality factors where the intrinsic damping was negligible. [46]. This system has been used to investigate the viscous and viscoelastic properties of simple liquids, including water, glycerol, and their mixtures [47,48].

Continuum mechanics theory was used to model the damping of acoustic vibrations of Au NPLs in homogeneous liquid environments, such as shown in Fig. 1a, where the top and bottom surfaces of Au NPLs were covered by the same fluid [49–51]. Following the previous theoretical analysis, the eigenvalue equation for the Au NPL vibrations in a viscous liquid is: [47,49].

$$2ic_s\rho_s\sqrt{p_f\left(c_f^2\rho_f-\mathbb{I}\omega\beta_f\right)}+\left(c_s^2{\rho_s}^2+\rho_f\left(c_f^2p_f-\mathbb{I}\omega\beta_f\right)\right)\tan\left(\frac{\hbar\omega}{c_s}\right)=0 \qquad (1$$

where h is the thickness of the Au NPL, c_s and c_f are the speed of longitudinal sound waves in the gold and fluid, and ρ_s and ρ_f are the density of the gold and fluid, respectively. $\beta_f = \kappa_f + 4\eta_f/3$ where η_f is the shear viscosity and κ_f is the bulk viscosity of the fluid. Eq. 1 is an eigenvalue equation that can be solved numerically to determine a complex angular frequency ω for the NPL vibrations. The frequency and quality factor of the breathing mode vibrations are then obtained by $f = \text{Re}[\omega]/2\pi$ and $Q = \text{Re}[\omega]/2lm[\omega]$. Fluid viscoelasticity can be included in this analysis by scaling the fluid viscosity by $\beta_f \rightarrow \beta_f/(1-i\lambda_f\omega)$, where λ_f is the structural relaxation time of the fluid [49]. When the structural relaxation time λ_f is comparable with the vibrational time scale $1/\omega$, fluid viscoelastic effects become significant. In contrast, the fluid only shows viscous damping effects if the relaxation time is λ_f is small. Previous analysis of Au NPLs in symmetrical liquid environments using Eq. (1) gave liquid relaxation times in good agreement with the literature [47, 49].

We extend the analysis of acoustic vibrations of Au NPLs to an inhomogeneous environment where the coverage of one of the surfaces was replaced by a bilayer membrane fluid, as shown schematically in Fig. 1b. Because the cellular fluid environment has a Brillouin frequency close to water (see Table 1), we assume that the cellular fluid can be treated as liquid water. Note that the vibrational amplitude of the acoustic mode is in the angstrom range and smaller than the thicknesses of the Au NPLs and the membrane [53]. Analysis of the system in Fig. 1 (b) gives the following eigenvalue equation (see Supporting Information for details).

Table 1

Biomechanical properties of mouse brain microvascular endothelial cells (bEnd.3) and human glioblastoma cells (LN-18). Number of Measurements N, Quality Factors Q for the Au NPLs with membrane damping, viscosity β of cell membranes, Brillouin oscillation frequencies f^B probed at 530 nm, and Elastic modulus of cell body E^b . Errors are 95% confidence limits.

	N	Q	β (× 10 – 3Pa·s)	f ^B (GHz)	E ^b (GPa)
bEnd.3	20	23.6 ± 1.1	24.4 ± 4.5	7.5 ± 0.1	2.2 ± 0.1
LN-18	38	26.2 ± 0.6	8.3 ± 1.9	7.4 ± 0.2	2.2 ± 0.1

adhesions would form on bare gold surfaces, as these structures generally appear where the cell membrane comes into contact with extracellular matrix proteins like fibronectin or collagen, or surface-assembled molecular layers [54,55]. Therefore, the contact mechanics driving the adhesion of the cell membrane to the gold surface are passive, involving van der Waals forces and other non-specific interactions [56].

2.2. Measuring structural relaxation times of membrane bilayers with high-frequency acoustic vibrations

$$c_{s}\rho_{s}\sqrt{\rho_{m}(c_{m}^{2}\rho_{m}-i\omega\beta_{m})}\left(\sqrt{\rho_{f}(c_{f}^{2}\rho_{f}-i\omega\beta_{f})}+\sqrt{\rho_{c}(c_{c}^{2}\rho_{c}-i\omega\beta_{c})}\right)$$

$$-i\left(\rho_{m}(c_{m}^{2}\rho_{m}-i\omega\beta_{m})+\sqrt{\rho_{f}(c_{f}^{2}\rho_{f}-i\omega\beta_{f})}*\sqrt{\rho_{c}(c_{c}^{2}\rho_{c}-i\omega\beta_{c})}\right)c_{s}\rho_{s}\tan\left(\frac{\omega\sqrt{\rho_{m}}d}{\sqrt{c_{m}^{2}\rho_{m}-i\omega\beta_{m}}}\right)$$

$$-i\left(c_{s}^{2}\rho_{s}^{2}+\sqrt{\rho_{f}(c_{f}^{2}\rho_{f}-i\omega\beta_{f})}*\sqrt{\rho_{c}(c_{c}^{2}\rho_{c}-i\omega\beta_{c})}\right)\sqrt{\rho_{m}(c_{m}^{2}\rho_{m}-i\omega\beta_{m})}\tan\left(\frac{\omega h}{c_{s}}\right)$$

$$-\left(\rho_{m}(c_{m}^{2}\rho_{m}-i\omega\beta_{m})\sqrt{\rho_{f}(c_{f}^{2}\rho_{f}-i\omega\beta_{f})}+c_{s}^{2}\rho_{s}^{2}\sqrt{\rho_{c}(c_{c}^{2}\rho_{c}-i\omega\beta_{c})}}\right)\tan\left(\frac{\omega\sqrt{\rho_{m}}d}{\sqrt{c_{m}^{2}\rho_{m}-i\omega\beta_{m}}}\right)\tan\left(\frac{\omega h}{c_{s}}\right)=0$$

$$(2)$$

Where d and h are the thickness of the membrane and Au NPL, c_m , ρ_m and β_m are the speed of sound, density and viscosity of the cell membrane, respectively, and c_c , ρ_c and β_c are the corresponding values for the cellular fluid. Solution of the above equation gives the frequency and quality factor of the breathing mode vibrations in the presence of the membrane. Note that our continuum mechanics model assumed a continuous and uninterrupted cell membrane that directly adheres to gold NPLs. It is unlikely that complex adhesion structures and focal

Understanding the molecular origins of liquid viscosity, such as the structural relaxation time, is fundamentally important and experimentally challenging [30,57–60]. Neutron, x-ray, ultraviolet and Brillouin scattering techniques have been used to probe the dynamics of liquids [7,27,29,30]. However, these methods are not applicable to the membranes of live cells. Recently, acoustic vibrations of metallic nanoparticles have been used to probe fluid viscoelastic properties through the vibrational mode damping [44,45,47,61,62]. The results show that

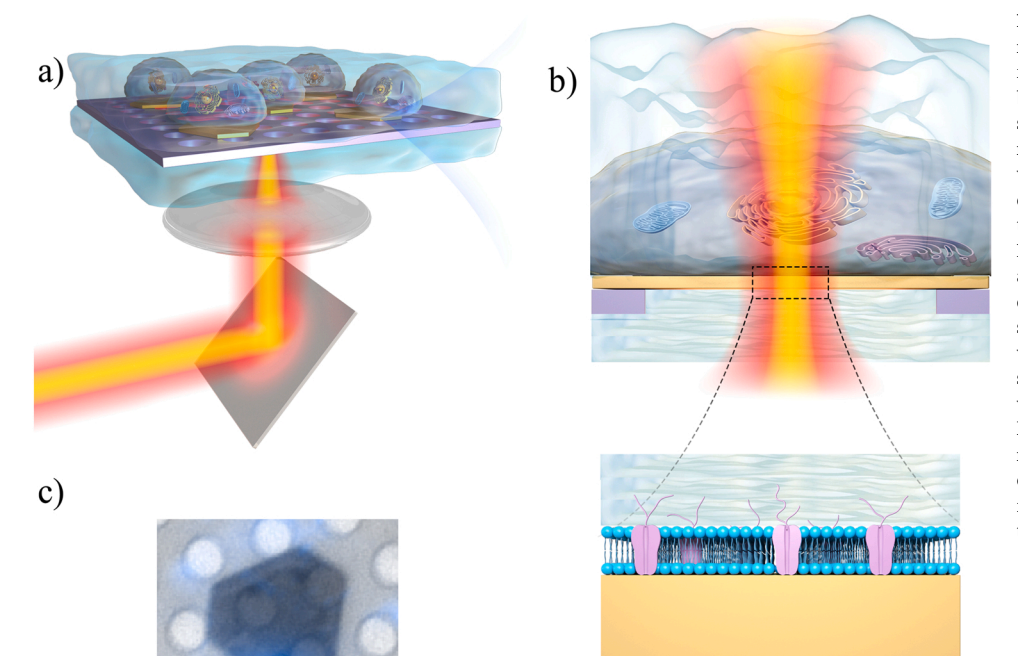


Fig. 2. Experimental setup for measuring viscoelasticity gigahertzmembrane at frequencies. (a) Schematic diagram showing biological cells growing on chemically synthesized Au NPLs deposited on a holey silicon nitride film. Optical pump and probe beams were focused on a suspended single Au NPL to excite and detect the acoustic vibrations through a 100 \times , 1.4 NA microscope objective. Note that the fixed cells were immersed in PBS, and the live cell experiments were in a cell culture medium. (b) A cross sectional view of a single cell adhering to a suspended Au NPL that was excited by a pump beam. The enlargement shows the details of Au NPL surfaces interfacing with cellular membrane and liquid. (c) A white light image of a single Au NPL on holey silicon nitride film overlaid with a fluorescence image of a cell nucleus stained with DAPI in blue. The image shows the successful culture of cells on the Au NPLs.

K. Yu et al. Photoacoustics 31 (2023) 100494

the acoustic modes exhibit frequency-dependent damping when interacting with simple liquids. At low vibrational frequencies, radiation of sounds waves is the dominant effect (inviscid limit) and damping is controlled by the acoustic impedance of the liquid. As the frequency increases, liquid viscosity effect becomes important, and the vibrational lifetimes start to decrease [48]. Finally, when the period of the vibrational motion approaches the liquid relaxation time, the vibration triggers a viscoelastic response in the liquid. At very high frequencies the liquid has an inviscid solid-like response, with an increased acoustic impedance compared to the results for the low frequency regime.

Two-dimensional Au NPLs were demonstrated to interrogate viscoelasticity in water and glycerol. Here we show that the gigahertzfrequency acoustic vibrations can be applied to probe membrane viscoelasticity in live cells, as shown schematically in Fig. 2a-b. Ultrathin Au NPLs with edge lengths of 10-20 µm and thicknesses of 20-30 nm were chemically synthesized and deposited on holey silicon nitride film (see Experimental Methods section for more details). The acoustic vibrations of the Au NPLs were excited by 800 nm pump pulses and detected by 530 nm probe pulses. Details about the experimental setup can be found elsewhere, and are briefly discussed in Experimental Methods section [46]. The reasons for suspending the Au NPLs over holey silicon nitride films were to reduce the radiation damping and, thus, improve the vibrational quality factors. This arrangement also simplifies the theoretical calculation in the continuum mechanics model. Biological cells were cultured on the holey silicon nitride film with suspended Au NPLs. The cells fully cover the film and were firmly attached on the Au NPLs. This was confirmed from fluorescence images, as shown in Fig. 2c, where the cell nucleus was fluorescently labeled. The measurements were performed on the suspended Au NPLs with cell growth on the top surface as illustrated in Fig. 2b. Consequently, the acoustic vibrations of the Au NPLs suffer damping from the liquid at the bottom surface, and the cellular membrane and cellular fluid on the top

Fig. 3a shows the vibrational quality factors of Au NPLs in phosphate-buffered saline (PBS) solution and also with mouse brain microvascular endothelial cell line (bEnd.3) attached to the nanoplates. Note that the cells were fixed and immersed in PBS buffer solution. The cell membranes lose their selective permeability in fixation and the cellular fluid becomes identical to PBS, [63] which is confirmed from the measured Brillouin frequencies as shown in Table S1. Experiments were done on ~ 40 Au NPLs and the acoustic vibrations have average

frequency of $f=69.3\pm4.3$ GHz. This corresponds to a NPL thickness of $h=24.8\pm1.7$ nm calculated by $h=c_s/2f$ (using the longitudinal speed of sound along the $\langle 111 \rangle$ direction of bulk gold of $c_s=3440m/s$). The vibrational quality factors are 26.6 ± 2 in PBS and 20.7 ± 1.5 for bEnd.3, where the errors are 95% confidence limits. PBS buffer is a water-based salt solution mainly containing disodium hydrogen phosphate and sodium chloride. The viscous properties of PBS are comparable to the water.

Next we calculate the structural relaxation times based on the fluid viscoelastic model. In the calculations, the parameters used for PBS were $\beta_f=4.05\times 10^{-3}\,$ Pa·s, $c_f=1750\,$ m/s and $\rho_f{=}1020\,$ kg/m³. For the membrane we used $\beta_m=25\times 10^{-3}\,$ Pa·s, $c_m=1900\,$ m/s and $\rho_m{=}1040 {\rm kg/m}^3$, and for the cellular fluid we used $\beta_c=4.05\times 10^{-3}\,$ Pa·s, $c_c=1510\,$ m/s and $\rho_c{=}1000 {\rm kg/m}^3$ (the same parameters as liquid water) (Data sources can be found in Table S1 in Supporting Information). Fig. 3b shows a plot of the calculated quality factors for PBS and cell membrane as a function of λ_f . The most noticeable feature of the calculated quality factors is that they are not monotonic: the quality factor values go through a minimum as a function of λ_f .

The minimum in the quality factor versus relaxation time plots has not been previously observed. This effect can be understood by considering the acoustic impedance of the fluid/membrane, and noting that larger values of the acoustic impedance of environment give smaller quality factors for the Au NPL. For the fluid (Fig. 3b) the effective acoustic impedance is given by $Z_f = c_f \rho_f \sqrt{1 - \frac{i\omega \beta_f}{c_f^2 \rho_f (1 - i\omega \lambda_f)}}$. At large values of λ_f , $Z_f \approx c_f \rho_f \sqrt{1 + \beta_f / \left(c_f^2 \rho_f \lambda_f\right)}$. In this limit Z_f decreases as λ_f increases, so the quality factors increase. In contrast, at small values of λ_f , $Z_f \approx c_f \rho_f \sqrt{1 + \frac{\omega^2 \beta_f \lambda_f}{c_f^2 \rho_f} - \frac{i\omega \beta_f}{c_f^2 \rho_f}}$. Now Z_f increases as λ_f increases, leading to a decrease in the quality factor. The different scaling of Z_f at large and small values of λ_f means that the quality factors must go through a minimum as a function of λ_f . Similar arguments hold for the membrane system. The obvious challenge is to determine the correct value of relaxation time.

To resolve this ambiguity, we note that there is a near linear correlation between viscosity and relaxation time for simple liquids, as shown in Fig. S6.[49] Theoretically two calculated values of λ_f can explain the experimental data for PBS in Fig. 3b: $\lambda_f = 0.9$ and $\lambda_f = 3.9$ ps, however,

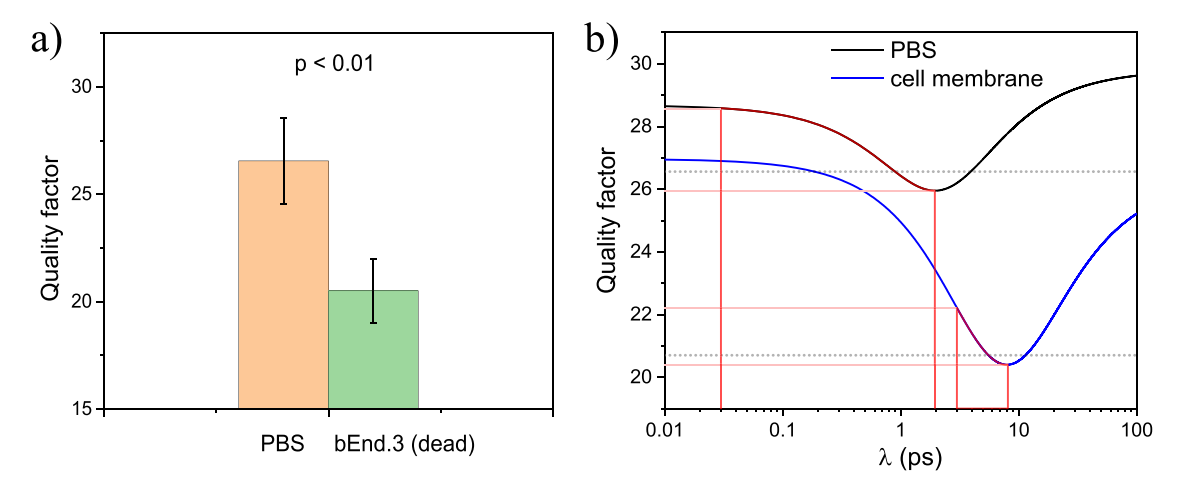


Fig. 3. Structural relaxation time of membrane bilayer fluid determined by acoustic vibrations of Au NPLs. (a) Quality factors of acoustic vibrations of Au NPLs in PBS buffer solution and with bEnd.3 cell membrane coating where the cells were fixed and immersed in PBS solution. The acoustic vibrations have average frequency of 69.3 ± 4.3 GHz and quality factors of 26.6 ± 2 in PBS, 20.7 ± 1.5 for bEnd.3. The errors are 95% confidence limits. Number of Measurements N = 40. The measured Brillouin frequency for the fixed cells is $f^B = 8.8 \pm 0.6$ GHz. (b) Plot of the vibrational quality factor as a function of λ_f for PBS buffer (black line), and the vibrational quality factor for bEnd.3 cell membrane using $\lambda_f = 0.9$ ps for the PBS fluid (blue line). The horizontal dotted lines in panel (b) are the measured average quality factors. The horizontal red lines show the statistic distributions of the measured quality factors, with corresponding derived relaxation times of 0.9 + 1/-0.9 ps for PBS, and 0.7 + 0.4/-0.7 ps for cell membrane.

only the $\lambda_f = 0.9$ ps value is assumed to be correct and realistic, because the properties of the buffer are close to those of water (which has a relaxation time of ca. 0.7 ps). We then consider the statistic distributions of the measured quality factors 26.6 ± 2 in PBS. When the O values increases, we can infer that the relaxation time should be decreasing, with a range of less than 0.9 ps, rather than increasing with a range greater than 3.9 ps. Similarly, when the Q value decreases and reaches the minimum of the curve, the relaxation time approaches the same value of 1.9 ps from both sides. In this case, we can still determine that the relaxation time should be within the range of 0.9-1.9 ps, rather than 1.9-3.9 ps. Keep decreasing the Q value is theoretically impossible. Therefore, we determined that the corresponding structural relaxation times of PBS is 0.9 + 1/-0.9 ps. Fig. 3b also shows the calculated quality factors for the bEnd.3 membranes versus λ_m using $\lambda_f = 0.9$ ps for the fluid. Again the experimental quality factors can be explained by two values of λ_m : 5.7 and 11.1 ps.

The analysis above yields the relaxation time for the membranes of $\lambda_m = 5.7$ and 11.1 ps. To the best of our knowledge there are no reported measurements of the compressible structural relaxation dynamics of cell membranes. We identify the correct structural relaxation time for the cell membrane by comparing the relaxation times to bulk liquid normal alkane. The cell membranes mainly contain lipids that are analogous to the linear alkane, tetradecane ($C_{14}H_{30}$), which is a simple hydrocarbon chain. The corresponding relaxation time for bulk C14H30 has been measured as 3 ps,[64] which is close to the 5.7 ps relaxation time from the continuum mechanics analysis. Furthermore, the choice of 5.7 ps also follows the linear correlation between viscosity and relaxation time in simple liquids, as shown in Fig. S6 in Supporting Information. Thus, we believe that the $\lambda_m = 5.7$ ps relaxation time is the correct choice for this system. Similarly, the derived structural relaxation times of cell membranes are 5.7 + 2.4 / -2.7 ps when considering the statistic distributions of the experimental data.

Previously, Nagao et al. had investigated the molecular dynamics in lipid bilayers using x-ray and neutron scattering spectroscopy.[30] The measured relaxation times are 30 and 500 ps. The faster relaxation was attributed to the rearrangements of the acyl tails, and the slower mode was associated with the motion of an entire lipid molecule escaping from the lipid bilayer. The molecular relaxations are dramatically different from the compressional measurements with the high-frequency acoustic vibrations. This implies that the motions detected in scattering measurements are not involved in membrane compressible viscoelasticity. Interpretation of the detailed molecular origin of the relaxation time presents an interesting avenue for future work.

2.3. Quantifying the viscosity of cell membranes at different cellular states

We extend the gigahertz-frequency viscoelasticity measurements to live cells. Mouse brain microvascular endothelial cells (bEnd.3) and human glioblastoma cells (LN-18) were cultured on the Au NPLs. The experimental results are shown in Table 1. The Au NPLs have vibrational frequencies of 60 ± 5 GHz and vibrational quality factors of 23.6 ± 1.1 and 26.2 ± 0.6 for bEnd.3 and LN-18 cells, respectively. Values for the membrane viscosity are not available for these systems, which means that there are two unknowns in the viscoelastic analysis (β_m and λ_m) and only one measurement (*Q*). Thus, to fit the experimental data the linear correlation between viscosity and relaxation time determined from literature data for water-glycerol mixtures was used to fix the relative values β_m and λ_m , see Supporting Information Fig. S6. The dependent β_m and λ_m values were then varied in the continuum viscoelastic model calculations to fit the experimental quality factors. This approach is justified by the good agreement of the values of β_m and λ_m for the fixed cells with the water-glycerol data. The calculated membrane viscosities determined from this analysis are $(24.4 \pm 4.5) \times 10^{-3}$ and $(8.3 \pm 1.9) \times$ 10^{-3} Pa·s with relaxation times of 5.4 +2.3/ -2.5 and 1.8 +0.8/ -0.9 ps for bEnd.3 and LN-18 cells, respectively. The results show that the

glioblastoma cells have membrane viscosities that are lower than the healthy endothelial cells by a factor of three. An increase in the fluidity of the membrane may be critical for cancer cell metastasis and provide a useful diagnostic biomarker for the assessment of cancer progression. Note that, the membrane viscoelasticity in bEnd.3 is similar for measurements in live cells and fixed cells, which indicates that the membrane structure stays intact during cell fixation.

Brillouin oscillations for the bEnd.3 and LN-18 cells are listed in Table 1. The measured frequencies are 7.5 \pm 0.1GHz and 7.4 \pm 0.2 GHz for bEnd.3 and LN-18 cells, respectively. Note that the Brillouin oscillation frequencies are close to that of water, which justifies the membrane model used to analyze the acoustic vibration data. The Brillouin wave has acoustic wavelength on the order of ~ 200 nm (for probing wavelength ~ 530 nm and cellular refractive index ~ 1.35), which is much larger than the membrane structure [7,33]. Thus, these measurements only interrogate the mechanical properties of cell body. The elastic modulus of cells calculated from the Brillouin oscillations frequency is 2.2 ± 0.1 GPa, which is consistent with previous measurements using Brillouin light scattering spectroscopy [34]. Note that the linewidth from the Brillouin spectrum is more sensitive than the frequency shift in differentiating cellular states. However, in our studies a high NA microscope objective was used to efficiently excite and probe acoustic vibrations of Au NPLs, which prevents accurate measurements of the attenuation of the Brillouin oscillations [65-68]. We have also demonstrated that the high-frequency acoustic vibrations provide better sensitivity in probing fluid viscous and viscoelastic properties than Brillouin waves [47].

It would be highly interesting to be able to differentiate cellular states by membrane biomechanics. Fig. 4 shows a color map of the vibrational quality factors calculated using Eq. 2 as a function of vibrational frequency and membrane viscosity, with relaxation times of $\lambda_f=1$, and $\lambda_c=0.65$ ps for culture medium, and cellular fluid, respectively. Higher membrane viscosities present stronger damping of the vibrational mode of Au NPLs. The measurements of the bEnd.3 and LN-18 cell membrane viscosities were also included in the figure. The significant difference in the viscosities of the bEnd.3 and LN-18 cell membranes indicate dramatic changes of membrane biomechanics in difference cellular states. Although Brillouin spectroscopy has been

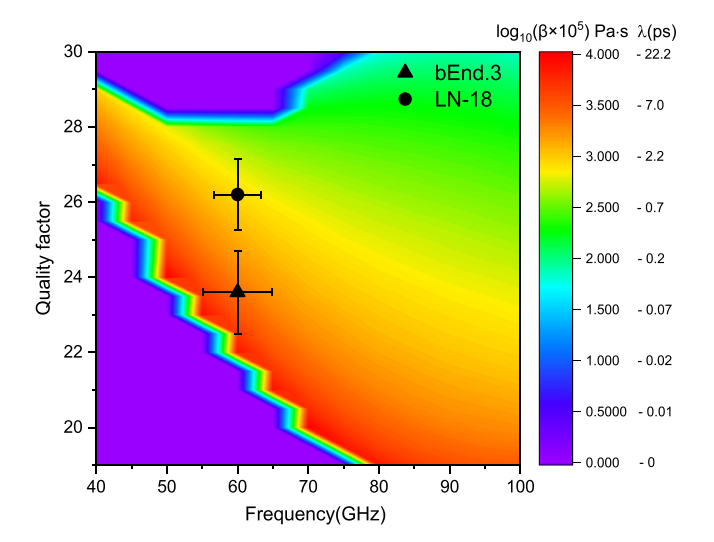


Fig. 4. Viscosity mapping of membrane fluid in live cells at different cellular states determined by the quality factors of high-frequency acoustic vibrations of Au NPLs. The markers show the experimental results for mouse brain microvascular endothelial cells (bEnd.3) and human glioblastoma cells (LN-18). Based on the viscoelastic model (Fig. 1b), the calculated membrane viscosities are $(24.4 \pm 4.5) \times 10^{-3}$ and $(8.3 \pm 1.9) \times 10^{-3}$ Pa·s for bEnd.3 and LN-18 cells, respectively. The cancerous cells exhibit a dramatic decrease of membrane viscosity compared to the normal cells.

demonstrated to differentiate the cancerous cells from normal cells, the direct probes of membrane viscoelasticity in the present measurements may provide exciting avenues in basic research to early diagnosis. Future challenges are obtaining a full understanding of the underlying complicated membrane mechanics at high frequencies [7,27]. We envision that high-frequency acoustic vibrations could be combined with molecular physics and cell biology to identify unique molecular fingerprints that control membrane viscoelasticity.

3. Conclusions

High-frequency biomechanics presents an interesting aspect of biophysics and has rarely been studied and associated with biology due to limited experimental techniques. Here, we investigate the cell membrane biomechanics at gigahertz-frequency using acoustic vibrations of Au NPLs by time-resolved pump-probe microscopy. Membrane damping of the acoustic vibrations has been accurately measured. The experimental results were modeled using a continuum mechanics theory. The analysis shows that the membranes in mouse endothelial cells have a viscoelastic response with an estimated structural relaxation time of ca. 5.7 + 2.4 / -2.7 ps. We further demonstrate that our membrane viscoelasticity measurements can be used to differentiate between the cancerous human glioblastoma cells (LN-18) and the normal mouse brain microvascular endothelial cells (bEnd.3). The viscosity of cancerous cells LN-18 is lower than that of healthy cells bEnd.3 by a factor of three. Further establishing the correlations between highfrequency biomechanics to cellular states and functions will be critical and beneficial for diagnosis and therapy.

4. Experimental methods

4.1. Materials

 $HAuCl_4\cdot 3~H_2O,$ 1-pentanol, Glycerol, CTAB, and PVP (Mw = 40,000) were purchased from Sigma-Aldrich. Ethanol was purchased from Sinopharm Chemical Reagent Co. Ultrapure water was used throughout the experiments. Holey silicon nitride films with pore size of $\sim\!5~\mu m$ were purchased from Ted Pella Inc. (catalog no. 21536). Mouse brain microvascular endothelial cell line (bEnd.3) and human glioblastoma cell line (LN-18) were used for investigations.

4.2. Au Nanoplates Synthesis

The Au NPLs were synthesized based on a previous method [47]. Briefly, a mixture of 1-pentanol (10 mL), PVP (Mw = 40,000, 30 mg) and water (600 mL) solution was prepared and heated to 110 °C. 50 μL HAuCl4·3 H2O (0.2 mM) was then added to the above solution. The reaction was kept at 110 °C for 2 h to facilitate the growth of Au NPLs. The yellow product was collected and washed with ethanol three times by centrifugation to remove excessive surfactants before drop-casting on the holey silicon nitride film. After Au NPLs were deposited on silicon nitride films, they were plasma cleaned for half an hour to remove the adsorbed surfactants on the surfaces of Au NPLs. This process is critical for the successful culture of live cells on Au NPLs. The Au NPLs synthesized in the current studies have surfaces with edge lengths of ~ 10 –20 μm and thicknesses of 20–30 nm.

4.3. Cell culture and treatment

Mouse brain microvascular endothelial cell line (bEnd.3) and human glioblastoma cell line (LN-18) were purchased from American Type Culture Collection (ATCC). Cells were cultured in Dulbecco's Modified Eagle's Medium (DMEM) supplemented with 10% fetal bovine serum (FBS) and 100 U/mL penicillin and 100 $\mu g/mL$ streptomycin in an incubator with 5% CO $_2$ at 37 °C. And cells were digested with 0.25% EDTA-trypsin and transferred to 3.5 cm cell culture dishes where the

silicon nitride films were put at the bottom to enable the cell attachment and growth. The growth of80–90% cell confluence on the film was ready for the optical experiment. Live cells were directly used for measurements or fixed with 100% methanol for 15 min at room temperature. For fluorescence imaging, the cells were incubated with antifading mounting buffer containing DAPI for nuclear staining.

4.4. Femtosecond transient absorption microscopy

The setup for transient absorption microscopy has been well described previously. A Coherent Mira 900 Ti:sapphire oscillator combined with a Coherent Mira optical parametric oscillator (OPO) laser system is used for the pump-probe measurements. The 800 nm pump beam from the Ti:sapphire oscillator was modulated at 1 MHz by an acousto-optic modulator (IntraAction AOM-402AF3), triggered by the internal function generator of a lock-in amplifier (Stanford Research Systems SR844). The probe beam from the OPO was tuned to 530 nm and overlapped with the pump beam and focused at a single Au NPL with an Olympus $100 \times$, 1.4 NA microscope objective. The delay time between the pump and probe beams was controlled by a Thorlabs DDS600 linear translation stage. The measurements were performed in reflection mode by monitoring the reflected probe beam intensity with an avalanche photodiode (Hamamatsu C12702-11) and the lock-in amplifier at a time constant of 30 ms. Typical powers were 5 mW for the pump and 100 µW for the probe. Under these conditions, the signal was stable, and no melting or reshaping of the Au NPLs was observed. The temperature rises of Au NPLs and cell membranes are $\sim 11~\text{K}$ and 4 K, respectively, at the center of the laser beam based on a twotemperature model (see the Supporting Information). Normally the membrane has a main transition temperature of ~ 20 °C [30]. Minor temperature increase above the transition temperature causes negligible change of membrane viscosity.

Acoustic vibrations of Au NPLs are excited in the pump-probe measurements. These acoustic vibrations cause periodic changes of the thickness of the Au NPL and thus of the absorption of the probe and consequently are detected by monitoring the probe beam intensity. A signal due to the propagating acoustic waves in the cellular fluid, known as Brillouin oscillations, is also detected. This signal arises from the interference between the reflected probe beams from the stationary surfaces and propagating acoustic waves in the fluid. The confined acoustic vibrations of Au NPLs detect the viscoelastic properties of cell membrane, while the Brillouin oscillations measure the viscoelastic properties of the cell body. Acoustic vibrations were measured three times at various locations for every cell on a suspended Au NPL, and the resulting quality factors were calculated by averaging the measurements. The Supporting Information includes a representative pumpprobe measurement curve, which was taken within a minute and includes both the breathing mode of Au NPLs and Brillouin oscillations. Fitting the curve with damped cosine functions gives the vibrational frequencies and lifetimes. These parameters are used for the characterizations of cell biomechanics.

Funding

This work is supported by National Key Research and Development Program 2022YFA1404500, the Natural Science Foundation of Guangdong (2020B010190001, 2022A1515011663), and the National Natural Science Foundation of China (12074266, 12074267). GVH acknowledges the support of the National Science Foundation through Award CHE-2002300.

Author contributions

KY and GW designed the experiments. YJ, YC conducted optical pump-probe experiments and data acquisition. HY, JC prepared the cell cultures. GH helped with the continuum mechanics model. YJ and KY

K. Yu et al. Photoacoustics 31 (2023) 100494

performed data analysis and wrote the paper with contributions from all the authors. GW supervised the entire project.

Declaration of Competing Interest

The authors declare that they have no competing interests.

Data Availability

All data needed to evaluate the conclusions in the paper are present in the paper and/or the Supporting Information. All data generated and analyzed during this study are available from the corresponding authors upon reasonable request.

Acknowledgments

None.

Appendix A. Supporting information

Supplementary data associated with this article can be found in the online version at doi:10.1016/j.pacs.2023.100494.

References

- [1] S.W. de Laat, P.T. van der Saag, M. Shinitzky, Microviscosity modulation during the cell cycle of neuroblastoma cells, Proc. Natl. Acad. Sci. U. S. A 74 (10) (1977) 4458–4461.
- [2] E.H. Barriga, R. Mayor, Adjustable viscoelasticity allows for efficient collective cell migration, Semin. Cell Dev. Biol. 93 (2019) 55–68.
- [3] S.J. Singer, G.L. Nicolson, The fluid mosaic model of the structure of cell membranes, Science 175 (1972) 720–731.
- [4] L.A. Bagatolli, J.H. Ipsen, A.C. Simonsen, O.G. Mouritsen, An outlook on organization of lipids in membranes: Searching for a realistic connection with the organization of biological membranes, Prog. Lipid Res. 49 (4) (2010) 378–389.
- [5] G.L. Nicolson, The fluid—mosaic model of membrane structure: still relevant to understanding the structure, function and dynamics of biological membranes after more than 40years, Biochim. Biophys. Acta - Biomembr. 1838 (6) (2014) 1451–1466
- [6] M. Cocchi, L. Tonello, F. Gabrielli, M. Pregnolato, Depression, osteoporosis, serotonin and cell membrane viscosity between biology and philosophical anthropology, Ann. Gen. Psychiatr. 10 (2011).
- [7] R. Prevedel, A. Diz-Muñoz, G. Ruocco, G. Antonacci, Brillouin microscopy: an emerging tool for mechanobiology, Nat. Methods 16 (10) (2019) 969–977.
- [8] A. Bonfanti, J.L. Kaplan, G. Charras, A. Kabla, Fractional viscoelastic models for power-law materials, Soft Matter 16 (26) (2020) 6002–6020.
- [9] W.J. Tyler, The mechanobiology of brain function, Nat. Rev. Neurosci. 13 (12) (2012) 867–878.
- [10] O.O. Adeniba, E.A. Corbin, A. Ganguli, Y. Kim, R. Bashir, Simultaneous timevarying viscosity, elasticity, and mass measurements of single adherent cancer cells across cell cycle, Sci. Rep. 10 (1) (2020) 12803.
- [11] Andrey S. Klymchenko, R. Kreder, Fluorescent probes for lipid rafts: from model membranes to living cells, Chem. Biol. 21 (1) (2014) 97–113.
- [12] S.-C. Lee, J. Heo, H.C. Woo, J.-A. Lee, Y.H. Seo, C.-L. Lee, S. Kim, O.-P. Kwon, Fluorescent molecular rotors for viscosity sensors, Eur. J. Chem. 24 (52) (2018) 13706–13718.
- [13] D.S. Heron, M. Shinitzky, M. Hershkowitz, D. Samuel, Lipid fluidity markedly modulates the binding of serotonin to mouse brain membranes, Proc. Natl. Acad. Sci. USA 77 (12) (1980) 7463–7467.
- [14] E. Evans, R. Hochmuth, Membrane viscoelasticity, Biophys. J. 16 (1) (1976) 1–11.
- [15] R.M. Hochmuth, P.R. Worthy, E.A. Evans, Red cell extensional recovery and the determination of membrane viscosity, Biophys. J. 26 (1) (1979) 101–114.
- [16] R.M. Hochmuth, K.L. Buxbaum, E.A. Evans, Temperature dependence of the viscoelastic recovery of red cell membrane, Biophys. J. 29 (1) (1980) 177–182.
- [17] T.T. Hormel, S.Q. Kurihara, M.K. Brennan, M.C. Wozniak, R. Parthasarathy, Measuring lipid membrane viscosity using rotational and translational probe diffusion. Phys. Rev. Lett. 112 (18) (2014), 188101.
- [18] S. Hénon, G. Lenormand, A. Richert, F. Gallet, A. New, Determination of the shear modulus of the human erythrocyte membrane using optical tweezers, Biophys. J. 76 (2) (1999) 1145–1151.
- [19] B. González-Bermúdez, G.V. Guinea, G.R. Plaza, Advances in micropipette aspiration: applications in cell biomechanics, models, and extended studies, Biophys. J. 116 (4) (2019) 587–594.
- [20] Y. Lefebvre, E. Leclerc, D. Barthès-Biesel, J. Walter, F. Edwards-Lévy, Flow of artificial microcapsules in microfluidic channels: A method for determining the elastic properties of the membrane, Phys. Fluids 20 (12) (2008), 123102.
- [21] Y.M. Efremov, T. Okajima, A. Raman, Measuring viscoelasticity of soft biological samples using atomic force microscopy, Soft Matter 16 (1) (2020) 64–81.

[22] N.A. Hosny, G. Mohamedi, P. Rademeyer, J. Owen, Y. Wu, M.-X. Tang, R. J. Eckersley, E. Stride, M.K. Kuimova, Mapping microbubble viscosity using fluorescence lifetime imaging of molecular rotors, Proc. Natl. Acad. Sci. U. S. A 110 (23) (2013) 9225–9230.

- [23] Y. Wu, M. Štefl, A. Olzyńska, M. Hof, G. Yahioglu, P. Yip, D.R. Casey, O. Ces, J. Humpolíčková, M.K. Kuimova, Molecular rheometry: direct determination of viscosity in Lo and Ld lipid phases via fluorescence lifetime imaging, Phys. Chem. Chem. Phys. 15 (36) (2013) 14986–14993.
- [24] L. Michels, V. Gorelova, Y. Harnvanichvech, J.W. Borst, B. Albada, D. Weijers, J. Sprakel, Complete microviscosity maps of living plant cells and tissues with a toolbox of targeting mechanoprobes, Proc. Natl. Acad. Sci. U. S. A. 117 (30) (2020) 18110–18118.
- [25] A.S. Kashirina, I. López-Duarte, M. Kubánková, A.A. Gulin, V.V. Dudenkova, S. A. Rodimova, H.G. Torgomyan, E.V. Zagaynova, A.V. Meleshina, M.K. Kuimova, Monitoring membrane viscosity in differentiating stem cells using BODIPY-based molecular rotors and FLIM, Sci. Rep. 10 (1) (2020) 14063.
- [26] M.S. Amin, Y. Park, N. Lue, R.R. Dasari, K. Badizadegan, M.S. Feld, G. Popescu, Microrheology of red blood cell membranes using dynamic scattering microscopy, Opt. Express 15 (25) (2007) 17001–17009.
- [27] S. Chakraborty, M. Doktorova, T.R. Molugu, F.A. Heberle, H.L. Scott, B. Dzikovski, M. Nagao, L.-R. Stingaciu, R.F. Standaert, F.N. Barrera, J. Katsaras, G. Khelashvili, M.F. Brown, R. Ashkar, How cholesterol stiffens unsaturated lipid membranes, Proc. Natl. Acad. Sci. U. S. A 117 (36) (2020) 21896–21905.
- [28] H. Hubrich, I.P. Mey, B.R. Brückner, P. Mühlenbrock, S. Nehls, L. Grabenhorst, T. Oswald, C. Steinem, A. Janshoff, Viscoelasticity of native and artificial actin cortices assessed by nanoindentation experiments, Nano Lett. 20 (9) (2020) 6329–6335.
- [29] E.G. Kelley, P.D. Butler, R. Ashkar, R. Bradbury, M. Nagao, Scaling relationships for the elastic moduli and viscosity of mixed lipid membranes, Proc. Natl. Acad. Sci. U. S. A. 117 (38) (2020) 23365–23373.
- [30] M. Nagao, E.G. Kelley, A. Faraone, M. Saito, Y. Yoda, M. Kurokuzu, S. Takata, M. Seto, P.D. Butler, Relationship between viscosity and acyl tail dynamics in lipid bilayers, Phys. Rev. Lett. 127 (7) (2021), 078102.
- [31] M. Krieg, G. Fläschner, D. Alsteens, B.M. Gaub, W.H. Roos, G.J.L. Wuite, H.E. Gaub, C. Gerber, Y.F. Dufrêne, D.J. Müller, Atomic force microscopy-based mechanobiology, Nat. Rev. Phys. 1 (1) (2019) 41–57.
- [32] M. Bailey, M. Alunni-Cardinali, N. Correa, S. Caponi, T. Holsgrove, H. Barr, N. Stone, C.P. Winlove, D. Fioretto, F. Palombo, Viscoelastic properties of biopolymer hydrogels determined by brillouin spectroscopy: a probe of tissue micromechanics, Sci. Adv. 6 (44) (2020) eabc1937.
- [33] F. Palombo, D. Fioretto, Brillouin light scattering: applications in biomedical sciences, Chem. Rev. 119 (13) (2019) 7833–7847.
- [34] J. Margueritat, A. Virgone-Carlotta, S. Monnier, H. Delanoë-Ayari, H.C. Mertani, A. Berthelot, Q. Martinet, X. Dagany, C. Rivière, J.-P. Rieu, T. Dehoux, High-frequency mechanical properties of tumors measured by brillouin light scattering, Phys. Rev. Lett. 122 (1) (2019), 018101.
- [35] T. Dehoux, M. Abi Ghanem, O.F. Zouani, M. Ducousso, N. Chigarev, C. Rossignol, N. Tsapis, M.-C. Durrieu, B. Audoin, Probing single-cell mechanics with picosecond ultrasonics, Ultrasonics 56 (2015) 160–171.
- [36] F. Pérez-Cota, R. Fuentes-Domínguez, S.L. Cavera, W. Hardiman, M. Yao, K. Setchfield, E. Moradi, S. Naznin, A. Wright, K.F. Webb, A. Huett, C. Friel, V. Sottile, H.M. Eisheikha, R.J. Smith, M. Clark, Picosecond ultrasonics for elasticity-based imaging and characterization of biological cells, J. Appl. Phys. 128 (16) (2020), 160902.
- [37] G. Antonacci, T. Beck, A. Bilenca, J. Czarske, K. Elsayad, J. Guck, K. Kim, B. Krug, F. Palombo, R. Prevedel, G. Scarcelli, Recent progress and current opinions in Brillouin microscopy for life science applications, Biophys. Rev. 12 (3) (2020) 615–624
- [38] S. Suresh, Biomechanics and biophysics of cancer cells, Acta Biomater. 3 (4) (2007) 413–438.
- [39] T. Lu, B. Anvari, Characterization of the viscoelastic properties of ovarian cancer cells membranes by optical tweezers and quantitative phase imaging, Front. Phys. 8 (2020)
- [40] A. Crut, P. Maioli, N. Del Fatti, F. Vallée, Acoustic vibrations of metal nano-objects: time-domain investigations, Phys. Rep. 549 (2015) 1–43.
- [41] G.V. Hartland, Optical studies of dynamics in noble metal nanostructures, Chem. Rev. 111 (6) (2011) 3858–3887.
- [42] M.A. van Dijk, M. Lippitz, M. Orrit, Detection of acoustic oscillations of single gold nanospheres by time-resolved interferometry, Phys. Rev. Lett. 95 (26) (2005), 267406
- [43] O.L. Muskens, N. Del Fatti, F. Vallée, Femtosecond response of a single metal nanoparticle, Nano Lett. 6 (3) (2006) 552–556.
- [44] D. Chakraborty, E. van Leeuwen, M. Pelton, J.E. Sader, Vibration of nanoparticles in viscous fluids, J. Phys. Chem. C. 117 (16) (2013) 8536–8544.
- [45] K. Yu, T.A. Major, D. Chakraborty, M.S. Devadas, J.E. Sader, G.V. Hartland, Compressible viscoelastic liquid effects generated by the breathing modes of isolated metal nanowires, Nano Lett. 15 (6) (2015) 3964–3970.
- [46] J. Wang, K. Yu, Y. Yang, G.V. Hartland, J.E. Sader, G.P. Wang, Strong vibrational coupling in room temperature plasmonic resonators, Nat. Commun. 10 (1) (2019) 1527.
- [47] K. Yu, Y. Yang, J. Wang, G.V. Hartland, G.P. Wang, Nanoparticle–fluid interactions at ultrahigh acoustic vibration frequencies studied by femtosecond time-resolved microscopy, ACS Nano 15 (1) (2021) 1833–1840.
- [48] K. Yu, Y. Jiang, C. Wright, G.V. Hartland, Energy dissipation for nanometer sized acoustic, Oscil., J. Phys. Chem. C. 126 (8) (2022) 3811–3819.

- [49] V. Galstyan, O.S. Pak, H.A. Stone, A note on the breathing mode of an elastic sphere in newtonian and complex fluids, Phys. Fluids 27 (3) (2015), 032001.
- [50] D. Chakraborty, J.E. Sader, Constitutive models for linear compressible viscoelastic flows of simple liquids at nanometer length scales, Phys. Fluids 27 (5) (2015), 052002
- [51] D. Chakraborty, G.V. Hartland, M. Pelton, J.E. Sader, When can the elastic properties of simple liquids be probed using high-frequency nanoparticle vibrations? J. Phys. Chem. C. 122 (25) (2017) 13347–13353.
- [52] R. Dimova, S. Aranda, N. Bezlyepkina, V. Nikolov, K.A. Riske, R. Lipowsky, A practical guide to giant vesicles. Probing the membrane nanoregime via optical microscopy, J. Phys. Condens Matter 18 (28) (2006) S1151–S1176.
- [53] A. Ahmed, M. Pelton, J.R. Guest, Understanding how acoustic vibrations modulate the optical response of plasmonic metal nanoparticles, ACS Nano 11 (9) (2017) 9360–9369.
- [54] P. Kanchanawong, G. Shtengel, A.M. Pasapera, E.B. Ramko, M.W. Davidson, H. F. Hess, C.M. Waterman, Nanoscale architecture of integrin-based cell adhesions, Nature 468 (7323) (2010) 580–584.
- [55] J. Enomoto, T. Kageyama, D. Myasnikova, K. Onishi, Y. Kobayashi, Y. Taruno, T. Kanai, J. Fukuda, Gold cleaning methods for preparation of cell culture surfaces for self-assembled monolayers of zwitterionic oligopeptides, J. Biosci. Bioeng. 125 (5) (2018) 606–612.
- [56] M.A. Ghanem, T. Dehoux, L. Liu, G.L. Saux, L. Plawinski, M.-C. Durrieu, B. Audoin, Opto-acoustic microscopy reveals adhesion mechanics of single cells, Rev. Sci. Instrum. 89 (1) (2018), 014901.
- [57] A. Yahya, L. Tan, S. Perticaroli, E. Mamontov, D. Pajerowski, J. Neuefeind, G. Ehlers, J.D. Nickels, Molecular origins of bulk viscosity in liquid water, Phys. Chem. Chem. Phys. 22 (17) (2020) 9494–9502.
- [58] F. Jaeger, O.K. Matar, E.A. Müller, Bulk viscosity of molecular fluids, J. Chem. Phys. 148 (17) (2018), 174504.
- [59] A.S. Dukhin, P.J. Goetz, Bulk viscosity and compressibility measurement using acoustic spectroscopy, J. Chem. Phys. 130 (12) (2009), 124519.
- [60] T.J. O'Sullivan, S.K. Kannam, D. Chakraborty, B.D. Todd, J.E. Sader, Viscoelasticity of liquid water investigated using molecular dynamics simulations, Phys. Rev. Fluids 4 (12) (2019), 123302.
- [61] T. Devkota, D. Chakraborty, K. Yu, G. Beane, J.E. Sader, G.V. Hartland, On the measurement of relaxation times of acoustic vibrations in metal nanowires, Phys. Chem. Chem. Phys. 20 (26) (2018) 17687–17693.
- [62] D. Chakraborty, B. Uthe, E.W. Malachosky, M. Pelton, J.E. Sader, Viscoelasticity enhances nanometer-scale slip in gigahertz-frequency liquid flows, J. Phys. Chem. Lett. 12 (13) (2021) 3449–3455.
- [63] U. Schnell, F. Dijk, K.A. Sjollema, B.N.G. Giepmans, Immunolabeling artifacts and the need for live-cell imaging, Nat. Methods 9 (2) (2012) 152–158.
- [64] T. Yamaguchi, Viscoelastic relaxations of high alcohols and alkanes: Effects of heterogeneous structure and translation-orientation coupling, J. Chem. Phys. 146 (9) (2017), 094511.

- [65] F. Perez-Cota, S. La Cavera Iii, S. Naznin, R. Fuentes-Dominguez, R.J. Smith, M. Clark, Apparent attenuation by opto-acoustic defocus in phonon microscopy, Photoacoustics 19 (2020), 100180.
- [66] E.G. Vitalyi, Contra-intuitive features of time-domain brillouin scattering in collinear paraxial sound and light beams, Photoacoustics 20 (2020), 100205.
- [67] T. Devkota, G. Beane, K. Yu, G.V. Hartland, Attenuation of acoustic waves in ultrafast microscopy experiments, J. Appl. Phys. 125 (16) (2019), 163102.
- [68] K. Yu, T. Devkota, G. Beane, G.P. Wang, G.V. Hartland, Brillouin oscillations from single au nanoplate opto-acoustic transducers, ACS Nano 11 (8) (2017) 8064–8071.



Kuai Yu received his Ph.D. in Physical Chemistry with Prof. Qing-Hua Xu at the National University of Singapore in 2013. He was then a postdoctoral researcher in Professor Hartland's group. In 2016, he started working at Shenzhen University, where he is currently an associate professor. His current research focuses on acoustic phonon strong coupling and the applications of acoustic vibrations.



Prof. Hartland obtained a Ph. D. from UCLA in 1991, and performed postdoctoral studies at the University of Pennsylvania with Prof. Hai-Lung Dai before joining the Department of Chemistry and Biochemistry at the University of Notre Dame in 1994. His research interests are in developing and applying novel spectroscopy techniques to study energy relaxation processes in single nanoparticles. Prof. Hartland is a Fellow of the AAAS, the American Chemical Society and the Royal Society of Chemistry.